Proceedings of ASME Turbo Expo 2011
GT2011
June 6-10, 2011, Vancouver, British Columbia, Canada

GT2011-45790

EXPERIMENTAL INVESTIGATIONS OF FLAME STABILIZATION OF A GAS TURBINE COMBUSTOR

Rainer Lückerath, Oliver Lammel, Michael Stöhr, Isaac Boxx, Ulrich Stopper, Wolfgang Meier
German Aerospace Center (DLR), Institute of Combustion Technology
Pfaffenwaldring 38-40, 70569 Stuttgart, Germany
e-mail: Rainer.Lueckerath@DLR.de

Bertram Janus, Bernhard Wegner
Siemens AG, Energy Sector, Fossil Power Generation Division
Mellinghofer Str. 55, 45473 Mülheim an der Ruhr, Germany

ABSTRACT

While today's gas turbine (GT) combustion systems are designed for specific fuels there is an urgent demand for fuel-flexible stationary GT combustors capable of burning natural gas as well as hydrogen-rich fuels in future. For the development of a fuel flexible, low-emission, and reliable combustion system a better understanding of the flow field – flame interaction and the flame stabilization mechanism is necessary. For this purpose, a down-scaled staged can combustion system provided with an optical combustion chamber was investigated in a high pressure test rig. Different optical diagnostic methods were used to analyze the combustion behavior with a focus on flame stabilization and to generate a comprehensive set of data for validation of numerical simulation methods (CFD) employed in the industrial design process.

For different operating conditions the size and position of the flame zone were visualized by OH^* chemiluminescence measurements. Additionally, the exhaust gas emissions (NO_x and CO) and the acoustic flame oscillations were monitored. Besides many different operating conditions with natural gas different fuel mixtures of natural gas and hydrogen were investigated in order to characterize the flashback behavior monitored with OH^* chemiluminescence.

For selected operating conditions detailed laser diagnostic experiments were performed. The main flow field with the inner recirculation zone was measured with two-dimensional particle image velocimetry (PIV) in different measuring planes. One-dimensional laser Raman spectroscopy was successfully applied for the measurement of the major species concentration and the temperature. These results show the variation of the local mixture fraction allowing conclusions to be drawn about the good premix quality. Furthermore, mixing effects of unburnt fuel/air and fully reacted combustion products are studied giving insights into the process of the turbulence-chemistry interaction and reaction progress.

Keywords: gas turbine combustion, fuel flexibility, high pressure test rig, laser diagnostic

INTRODUCTION

Modern gas turbines like the SGT5-8000H [1] are designed to deliver highest performance and reliability while meeting strict requirements with respect to emissions. While natural gas is the most commonly used fuel today, fuels containing high amounts of hydrogen are expected to become more important in the future. This poses increased demands on the design to ensure stable operation not only by optimizing designs for a single fuel type, but to come up with highly fuel-flexible combustion systems. The development of such fuel-flexible combustion systems requires a detailed understanding of flame stabilization mechanisms as well as simulation tools able to capture the underlying flow and combustion phenomena. Detailed experimental investigation using advanced laser diagnostics is a suitable way to obtain both understanding and provide a basis for validation of computational fluid dynamics (CFD) based combustion models.

For the investigations presented here, a down-scaled industrial GT staged can combustor was installed in the high

pressure test rig at the Institute of Combustion Technology of the German Aerospace Center (DLR) in Stuttgart and operated at a pressure of 4 bar and thermal power of up to 1.2 MW. A combustion chamber with quartz windows and large optical ports in the test rig allowed the application of optical and laser measuring techniques. The combustor was operated with natural gas and preheated air and the operating conditions were varied in a wide range of fuel staging, equivalence ratio, thermal power and addition of hydrogen to the fuel. Here, OH^* chemiluminescence imaging, particle imaging velocimetry (PIV), and one-dimensional Raman scattering were applied in combination with exhaust gas analysis and dynamic pressure recording. Of particular interest was the interaction between the central pilot flame and the surrounding main burners.

The high intensity of the OH^* chemiluminescence indicates the region of the flame zone and the integral intensity is a measure for the heat release rate [2, 3]. With PIV, the two components of the flow velocity in the measuring plane were determined to get 2-dimensional velocity fields. One-dimensional laser Raman scattering was used to quantitatively measure the major species concentrations (N_2, O_2, H_2O, C_xH_y, CO_2, CO and H_2) together with the temperature. By this technique, the local mixture fraction and the reaction progress could be determined, identifying effects of unmixedness and turbulence-chemistry interactions [4].

In this paper, the general experimental setup and the measurement systems are presented and a few selected experimental results are shown and discussed. The main goals of the investigations were to provide a better understanding of the flame behavior and the generation of an extensive data base for the validation of numerical simulations used in the industrial design process.

EXPERIMENTAL SET-UP

Burner and Combustion Chamber

A staged can combustion system with eight main swirl burners arranged on a circle and a pilot swirl burner with a cone in the center [1] was downscaled by a factor of 0.3 to fit into the high pressure test rig of the DLR in Stuttgart. The original fuel staging with five different fuel injections was reduced to two lines for the injection in the swirler vanes of the mains and the pilot. To start the flame an ignition burner was used located in the centre of the pilot burner. The burner used in these experiments is shown in Fig. 1 through a window of the combustion chamber.

Originally, the combustion chamber had a cylindrical shape, but for the application of laser diagnostic methods plane windows are preferred. Therefore, a square cross section of the combustion chamber was chosen. Although this change certainly has implications for some aspects of the flow structure in the combustion chamber the impact was thought to be limited on the central region of the pilot flame and its interaction with the main flame in the direct wake of the pilot

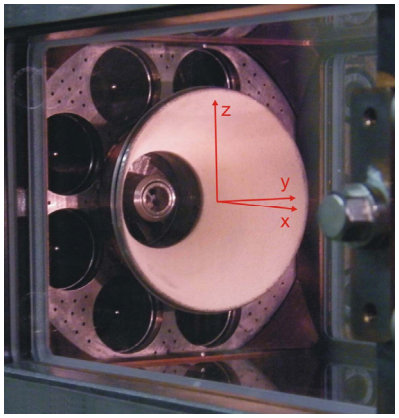

Figure 1. The downscaled combustor with 8 main swirl burners and the pilot swirl burner with its cone. The used coordinate system is also indicated.

cone. The length of the combustion chamber was 380 mm and the cross section was 95 x 95 mm². On each of the 4 sides the combustion chamber was equipped with 2 sections of double-glazed windows with cooling air flowing between the glass plates. For the optical diagnostics the quartz windows of the section close to the burner were used yielding access to a length of 155 mm of the combustion chamber (see Fig. 2). The second section was also made of quartz windows in order to have similar thermal boundary conditions over the entire wall of the combustion chamber. This choice was made primarily to provide simple definition of boundary conditions in CFD validation cases to be calculated later for the burner and rig. The exit of the combustion chamber had a conical shape with a length of 154 mm and a minimum diameter of 62 mm. A hole in the upper wall of the combustion chamber in the bar between the two window sections was used for the measurements of the pressure dynamics (compare Fig. 2).

The combustion air was preheated to temperatures of T_{air} = 667 – 704 K, whereas the fuel was not preheated. The burner was operated at a pressure of p = 4 bar with a maximum thermal load of P_{therm} = 1.2 MW.

The coordinate system in the combustion chamber is defined as *x* gas flow direction, *y* horizontal axis and *z* vertical

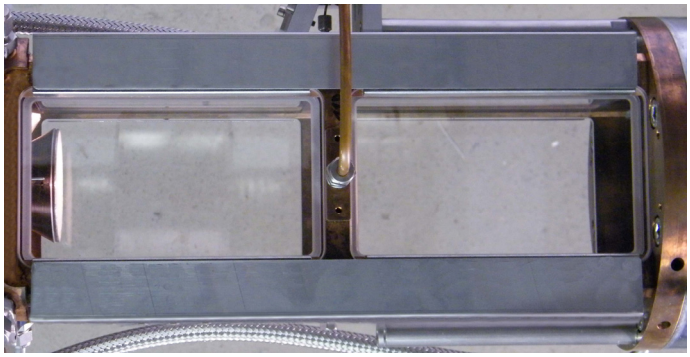

Figure 2. Optical combustion chamber with two sections of windows. The pilot cone is seen on the left side.

axis as shown in Fig. 1. The origin is located at the end of the pilot cone (x = 0 mm) and on the combustor axis (y = 0 mm, z = 0 mm).

High Pressure Test Rig

The burner and the combustion chamber were horizontally mounted in the pressure vessel of the high pressure test rig. Through large windows in the pressure vessel a good optical access to the first section of the combustion chamber was achieved. The electrically preheated air was directly fed to the burner where it was divided into pilot air and main air. An additional cold air line was used to cool the windows. The natural gas used as fuel had a typical composition of 95.9% CH_4, 2.4% C_2H_6, 0.6% C_3H_8, 0.9% N_2, and 0.1% higher hydrocarbons. The mass flow rates of fuel and air were measured by Coriolis flow meters with an accuracy of about 1%. Several pressure transducers recorded the pressure in the combustion chamber and the pressure drop at the burner. A suction probe behind the combustion chamber enabled the measurement of the concentrations of NO, NO_2, CO, CO_2, and O_2 and the exhaust temperature was measured at the same location with a thermocouple. The data logging system of the test facility recorded every 5 s values of the concentrations and all relevant information about the operation of the burner like mass flows, temperatures and pressures. Additional information to the high pressure test rig can be found in [5].

Operating Conditions

The burner was operated at more than 40 different operating conditions for baseload conditions at 4 bar with thermal power of P_{therm} = 1.0 – 1.2 MW. The operating condition with an air equivalence ratio λ, i.e. the reciprocal of the equivalence ratio Φ, of λ_{global} = 1.86, T_{air} = 704 K, P_{therm} = 1.1 MW, p = 4 bar was defined as the reference operating condition. The fuel was not preheated but reached in the burner a temperature of $T_{fuel\_main} \approx 363$ K and $T_{fuel\_pilot} \approx 553$ K due to a preheating effect by the contact of the fuel tubes with the hot air upstream the burner. Compared to this reference operating condition, several parameters were varied covering the relevant space of operating conditions for the actual combustion system:

- The fuel split between pilot and main burners was changed by reducing the pilot fuel down to 67% at constant total fuel mass flow.
- The global equivalence ratio was varied within a small range corresponding to a variation of the adiabatic flame temperature T_{ad} of ±40 K which is a typical variation for baseload conditions. Moreover, experiments for partload relevant conditions with lower flame temperatures were performed but not discussed in this paper.
- The total mass flow was reduced by up to 10%.
- Up to >40%$_{vol}$ H_2 was added to the natural gas in the main fuel mass flow. The mixture of natural gas with hydrogen was achieved by substituting a part of natural gas by hydrogen resulting in the same adiabatic temperature.

In this paper, results of some selected baseload operating conditions are discussed. Parameter variations were performed around the centre point mainly in an orthogonal manner, but also including a few diagonal points as well.

Purpose of the parameter variation was a thorough characterization of the combustion system under investigation to make proper choice for operating conditions with more detailed investigation in the next step. For each operating condition a general characterization was performed including measurement of the emissions of the exhaust gases, the detection of acoustic flame oscillations, and the visualization of the flame shape and position with OH^* chemiluminescence. For selected operating conditions additional optical techniques were applied: high-speed OH^* chemiluminescence imaging, velocity field measurements by PIV and the determination of major species concentration including temperature by one-dimensional laser Raman spectroscopy.

The reference operating condition showed stable combustion with low emissions whereas near the lean blow-off limit of the pilot burner the combustor exhibited acoustic oscillations combined with higher CO emissions.

Measuring Techniques

During the experiments different diagnostics methods were performed. As standard techniques OH^* chemiluminescence, exhaust gas composition, and dynamic pressure were recorded for all operating conditions. For selected operating conditions the more complex laser diagnostic methods particle image velocimetry and one-dimensional laser Raman spectroscopy were applied.

OH^* Chemiluminescence (OH^*-CL): For the measurement of the OH^* chemiluminescence (CL) an intensified CCD camera fitted with an 64 mm UV lens (f/2, Halle Nachf.) and a UV ($\lambda \approx 312 \pm 20$ nm) interference filter were used. The signal intensity of the OH^* chemiluminescence depends on the concentration of the electronically excited OH^* radicals, which are formed by chemical reactions, predominantly via $CH + O_2 \rightarrow CO + OH^*$ [6]. Due to the short lifetime of OH^* the chemiluminescence originates only from the reaction zone. Therefore, this technique yields information about the size and position of the flame zone [2]. The signal was detected with a gate time of 40 µs. For all series 200 single instantaneous images were recorded with a repetition rate of 3.3 Hz and averaged. Because the signal from the entire combustion chamber was collected by the camera the signals were spatially integrated in the depth (line of sight).

For the OH^*-CL series with high-speed detection 3000 single instantaneous images were recorded with an intensified high-speed CMOS camera (LaVision HighSpeedStar with HighSpeedIRO) with a repetition rate of 3 kHz and a gate time of 40 µs. A f/1.8 UV camera lens with a focal length of 45 mm was used together with a UV ($\lambda \approx 319 \pm 22$ nm) interference filter.

The view of the cameras was through one side window with the burner on the left side (compare left window in Fig. 2). The images of the OH^*-CL cameras covered the complete 90 mm height of the window. The length of the image is about 155 mm so that the first part of the combustion chamber is seen. The exit planes of the main and pilot swirl burners are approximately 42 mm and 30 mm outside the images, respectively, whereas the pilot cone is visible and marked in the CL images. The CL images are displayed with different scaling factors to take advantage of the full dynamic range of the color bar. A scaling factor of e.g. "x1.5" given in the CL images indicates that the maximum of the color bar was multiplied by a factor of 1.5. This means that a larger scaling factor is used for a stronger signal.

Emissions: The exhaust gas composition sucked with the probe behind the combustion chamber was analyzed to get information on the emissions. The NO and NO_2 concentrations were determined by means of UV absorption (ABB Limas 11), the CO and CO_2 concentrations by IR absorption (ABB URAS 14), and the O_2 concentration by paramagnetism (ABB Magnos 16) at dry conditions. All concentrations of NO_x (NO, NO_2) and CO were normalized to 15% O_2. The measured data recorded every 5 seconds were averaged for the time interval of stable operating conditions. The calculated standard deviation is given in the drawing as the vertical bar.

Pressure Recording: The dynamic pressure was measured at the top wall of the combustion chamber between the two sections of windows and in the plenum of the main swirlers with piezoelectric pressure transducers and evaluated by fast Fourier transformation (FFT) once per second. There was no significant difference found between the two different measuring positions. The data shown in this paper originate from the combustion chamber. The small and narrow peaks at 50 Hz and all odd-numbered multiples of 50 Hz are due to an interference with the 50 Hz line frequency.

Particle Image Velocimetry (PIV): Two-component velocity fields in different vertical planes in the combustion chamber were measured with particle image velocimetry (PIV). The planes were chosen with a main focus on the task of CFD validation picking locations of common interest or attempting to capture regions with strong gradients thought to be of relevance for the overall flame stabilization (e.g. the shear layer between the main and pilot stages). The set-up consisted of a dual-cavity flashlamp pumped frequency doubled Nd:YAG laser (New Wave Solo PIV 120) with a laser pulse energy of 120 mJ at a pulse duration of 5 ns. The two laser beams were formed with two cylindrical lenses (f_1 = -12.7 mm, f_2 = 200 mm) and a spherical lens (f_3 = 1000 mm) to a light sheet with a width of about 140 mm and a thickness of approx. 1 mm and guided with mirrors vertically through the combustion chamber. With a delay between the two laser pulses of 7 µs to 9 µs the particles (titanium dioxide, nominal diameter 1 µm) were illuminated twice. The scattered light was collected with a camera lens (f = 50 mm, f/5.6) and recorded with a CCD camera with a repetition rate of 5 Hz. The particles were seeded to the main and the pilot air. From the displacement in the two images the instantaneous velocity fields were calculated and averaged. The spatial resolution of 4 × 4 mm² resulted from the interrogation window size of 32 × 32 pixels. All these volumes are overlapping by 50% resulting in information every 2 mm in x and z direction.

During the measurements the windows of the combustion chamber were covered with particles resulting in increasing stray light. After approximately 15 minutes the burner was shut down and the windows had to be cleaned or replaced. A more detailed description of the set-up and the data evaluation is found in Ref. 7.

One-Dimensional Laser Raman Spectroscopy: The fundamentals of laser Raman spectroscopy for flame investigations can be found in the literature [8, 9]. At DLR, a unique laser system was designed for Raman experiments at test rigs [4, 10]. It consists of three double-pulse Nd:YAG lasers (Spectra-Physics PIV-400, frequency-doubled to 532 nm, 5 × 300 mJ pulse energy, one resonator out of operation, 7 ns pulse duration each). Due to the naturally low quantum efficiency of the Raman scattering process, high laser pulse energies have to be used for single-shot measurements. But the high power density can damage the combustor windows. Therefore, the five pulses are emitted with short delay times of about 50 ns between the single peaks. Additionally, they pass a pulse stretching unit reducing the peak power of the pulse to a fifth of the original value while the complete pulse energy is nearly maintained. The whole laser system is integrated in two temperature stabilized mobile containers enabling the application of the Raman technique at test rig facilities. The complete diagnostic setup is shown in Fig. 3.

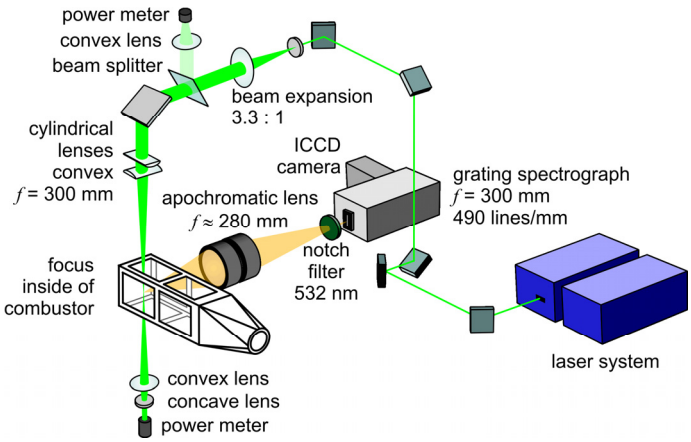

Figure 3. Experimental setup for one-dimensional laser Raman spectroscopy.

After an expansion of the laser beam to a diameter of about 40 mm, it passed through the focusing optics consisting of two

cylindrical lenses which were oriented perpendicular towards each other. This astigmatic arrangement is used to avoid an interfering plasma breakdown in the laser focus, because a stretched focus with a much lower energy density than a simple point-focus is generated.

To determine the pulse power at the measuring position the pulse power was measured with detector heads of a power meter in front of and behind the pressure vessel. With these two measured pulse powers the reduction by several beam forming devices, the windows of the pressure vessel and impurities on the combustor windows could be estimated.

The scattered light from the focus was collected at 90° with a large f/2 apochromatic lens system that relayed about 8 mm of the focal region of the laser beam onto the entrance slit of a grating spectrograph (Acton Research SpectraPro 300i, f = 300 mm, 490 lines/mm, f/4, dispersion ~6 nm/mm). The magnification of the detection optics was 1.76. A holographic notch filter in front of the spectrograph blocked the Rayleigh scattered light and the stray light at 532 nm. The spectrally dispersed image of the beam was captured by an intensified CCD camera (Princeton Instruments PI-Max, 1340 × 1300 pixels, 26.8 mm × 26 mm chip size) equipped with a fiber-coupled image intensifier (Gen III, GaAs photocathode). By applying a hardware binning of the pixel intensities it was possible to lower the effect of readout noise. The 1D measurement volume with a length of 8 mm was divided into 14 cells each with a length of 0.57 mm and diameter of ~0.5 mm according to the diameter of the laser beam in the observed section. The 14 spectra from these cells were recorded simultaneously.

The whole diagnostic setup (except for the containers housing the laser system) was built on computer controlled 3D translation stages. This made it possible to scan the 98 different spatial locations with short time delays. All these measuring positions were placed on a horizontal plane with z = 0 mm. With a repetition rate of 10 Hz the concentrations of the major chemical species (CO_2, O_2, CO, N_2, C_xH_y, H_2O, H_2) were measured which were used to calculate the temperature and the mixture fraction [11].

Extensive calibration measurements are indispensable for the correct analysis of the raw data. For this purpose, different calibration measurements using an electrical gas heater and a custom-built matrix burner were performed in the combustion chamber mounted in the high pressure test rig to obtain the same optical boundary conditions. The temperature and the chemical composition of different heated gas flows as well as flat laminar CH_4/air and H_2/air flames with known exhaust gas temperatures were measured.

Both, statistical and systematic error, depend on numerous different influences, e.g. the window opacity or the laser beam alignment. Therefore, the error values can vary significantly from one measurement day to the other. Under very good conditions, the uncertainty of a single-shot temperature measurement in hot reaction products was 6.2 % (standard deviation). A lower limit for the systematic error of the temperature is given by the accuracy of the CARS measurements (~ 3%) that were used for the calibration of the system. The total error (quadratic sum of statistical and systematic error) of the single-shot temperature measurement in hot reaction products can therefore be estimated to approximately 7% in the best case. A worst case estimation results in a total error of 15%.

Analysis of the Raman Raw Data: The raw data acquired by the 1D Raman system consisted of image files with a spectral resolution in the horizontal and a spatial resolution in the vertical direction. The quantitative data evaluation of these images was based on the comparison of the Raman signals from the GT flames with signals from the calibration measurements.

The pre-processing of the data included several image processing steps (spectral shift correction, background subtraction), intensity normalizations (laser pulse energy, intensifier gain, day calibration) and the channel binning, which determined the spectral band intensities from the corrected images. The last pre-processing step was an intensity filter for the elimination of interfering signals generated by laser-induced plasma-breakdowns.

After the pre-processing, the thermochemical information was extracted by analyzing the intensities of the species channels. The major challenge of this evaluation was to correct the error that is produced by overlapping spectral bands (‘channel crosstalk’) and to convert the signal intensities into absolute number density values. For this purpose, cross-talk coefficients and calibration coefficients had to be known. They were determined in advance by analyzing the calibration measurements.

Unfortunately, some interfering effects, like the increasing opacity of the combustion chamber windows due to the strong heat load, made it necessary to use additional correction routines that scaled the intensity of the pre-processed species channels in order to match the mean temperature of the unburnt fuel/air mixture with the mixing temperature that was calculated based on thermocouple measurements. For measurements without samples of unburnt reactants, this intensity scaling factor was inter- or extrapolated. Another pixel-row dependent intensity scaling routine had to be used in order to make sure that the samples from the 14 observation volumes provided identical mean temperature values after ensemble averaging.

RESULTS

Different examples of the results are discussed in this paper. First, the dependence of the emissions and of the flame position on the fuel split between pilot and main burners is shown. The pilot fuel flow was reduced until the flame became unstable near the lean blow off limit of the pilot burner. Further, the combustion behavior at the reference operating

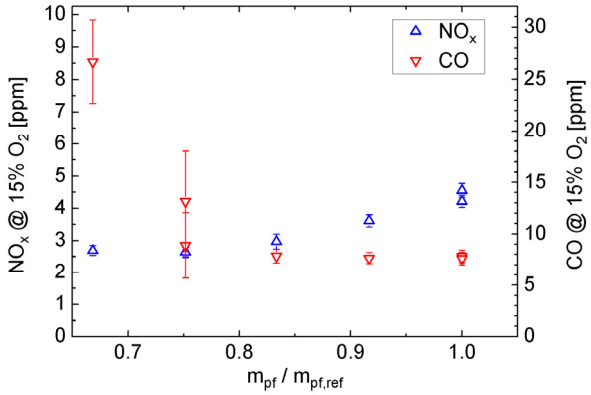

Figure 4. NO_x and CO emissions versus the relative fuel mass flow of the pilot burner. The vertical bars represent the standard deviation.

condition is analyzed on the basis of the PIV and Raman measurements. Finally, the results obtained with different fuel mixtures of natural gas and hydrogen are presented.

Variation of Fuel Split

Starting from the reference operating condition the fuel split between pilot and main burner was varied by reducing the mass flow of the pilot fuel with constant total fuel mass flow. When the fuel mass flow of the pilot burner, m_{pf}, was reduced compared to the reference mass flow, $m_{pf,ref}$, to a value of $m_{pf}/m_{pf,ref} = 0.75$ the flame started to become instable. This can be seen in Fig. 4 by the increase of the CO emissions and also of the CO standard deviation (shown as vertical bars) for pilot fuel mass flows of $m_{pf}/m_{pf,ref} \leq 0.75$ in comparison to the reference.

In Fig. 5 the OH^* chemiluminescence images of the series with different fuel splits are presented. The averaged images (left) and the RMS images (right) are shown for the reference operating condition in the upper row and for reduced pilot fuel mass flows as indicated on the left side. The reason for the moderate asymmetry visible in the images is unclear. At the reference condition, the flame is anchored near the exit of the cone of the pilot burner. This becomes even more obvious after "eliminating" the line-of-sight integration of the signal. With the assumption of cylindrical symmetry an Abel deconvolution of the OH^*-CL images was performed resulting in the chemiluminescence distribution in the central vertical plane y = 0 mm. For the reference case, the corresponding distribution is displayed in Fig. 11f. Here it is seen that the flame is restricted to an area confined by the cone and the downstream projection of the cone. Near the flame axis, there is hardly any combustion. It is shown later, that this region lies within the central recirculation zone. Outside the cone and its downstream projection, no flame reactions are observed. The flame anchoring region is thus restricted to a small area where the conditions for flame stabilization are favorable. It will be shown later that the flow velocities are relatively low in this region and that here unburnt fuel/air compositions from the main burners are mixed into the hot exhaust gas from the pilot flame. The RMS fluctuations of Fig. 5 demonstrate that the heat release is subject to significant variations in this area.

Decreasing the pilot fuel mass flow at constant λ_{global} leads to a drastic reduction of the heat release close to the pilot burner cone. The flame is no longer anchored near the exit of the cone. Further downstream, the size and position of the main heat release zone are not significantly changed, but the fluctuation in this area is considerably higher compared to the reference operating condition. This is an indication for a fluctuating heat release rate due to thermo-acoustic instabilities at lean pilot burner conditions, especially for $m_{pf}/m_{pf,ref} = 0.67$ which is close to the lean blow off limit of the pilot burner and thereby also of the main burners.

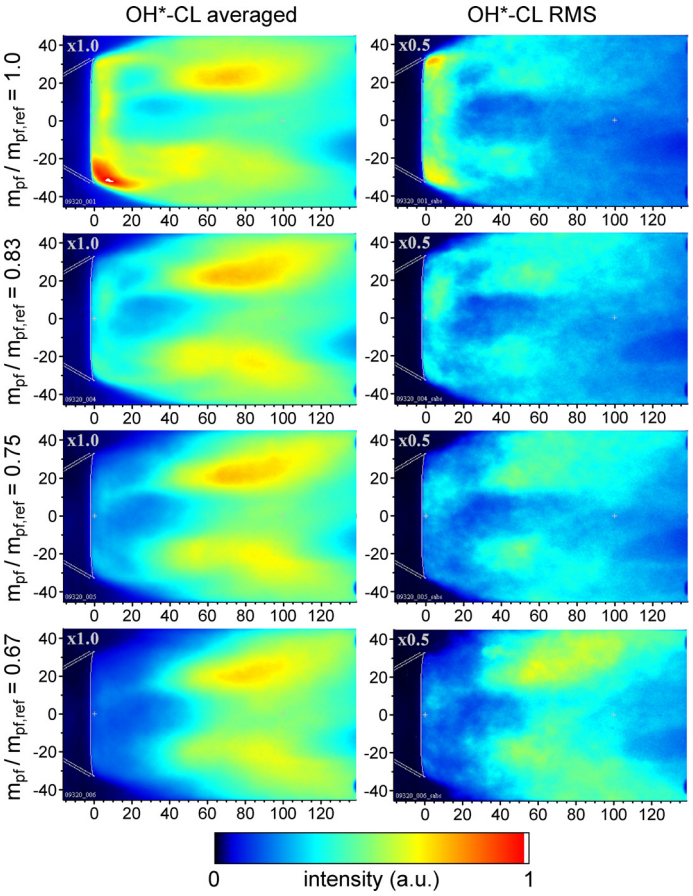

Figure 5. OH* chemiluminescence images (left: averages, right: RMS) for different fuel splits as indicated on the left side of the images.

Dynamic Processes

For a more detailed study of the instabilities at lean pilot conditions for $m_{pf}/m_{pf,ref} = 0.75$ a frequency spectrum was calculated from the reading of the pressure transducer by FFT, as drawn in Fig. 6. Here, a strong peak is found at approximately 117 Hz which shows a RMS amplitude of the pressure fluctuation of about 2% relative to the absolute

pressure in the combustion chamber. For the stable reference operating condition only broader structures with amplitudes less than 0.2% similar to the spectrum of Fig. 6 but without the peak at 117 Hz were found. Otherwise, changing the operation to leaner conditions with $m_{pf}/m_{pf,ref}$ = 0.67 resulted in an increase of the amplitude of the peak by a factor of 1.5 – 2.

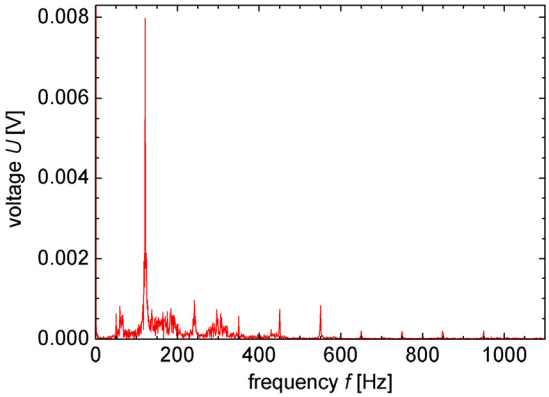

Figure 6. Pressure dynamics for the operating condition with $m_{pf}/m_{pf,ref}$ = 0.75.

High-speed imaging with a frame rate of 3 kHz were used to detect the time resolved variation of OH*-CL intensities. In Fig. 7 a series of 30 consecutively recorded images is shown. Starting with low CL intensity of the first images in Fig. 7 the integrated intensity increases with time as seen in the following images reaching the maximum in the 20th image. The following decrease of the intensity is faster than the increase. This variation of the integrated intensity is explained by an oscillating heat release rate. Plotting these integral intensities of many images versus time results in the curve in Fig. 8. The

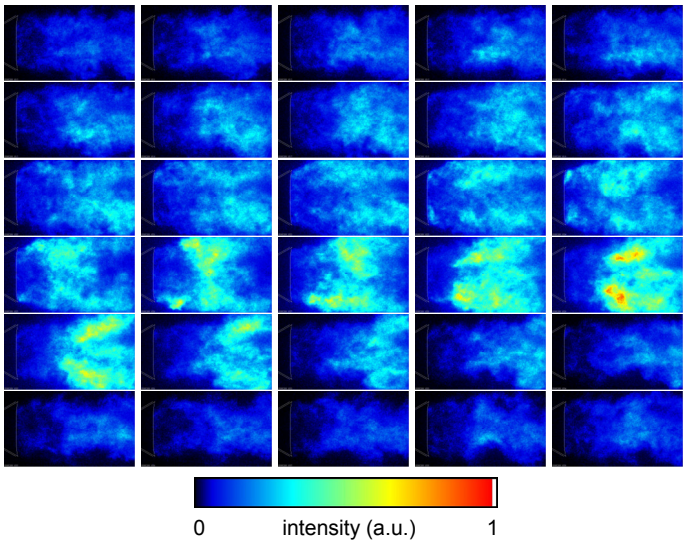

Figure 7. A series of high-speed OH*-CL images showing the periodical variation of heat release for the operating condition with $m_{pf}/m_{pf,ref}$ = 0.75. The time between two images is Δt = 0.333 ms.

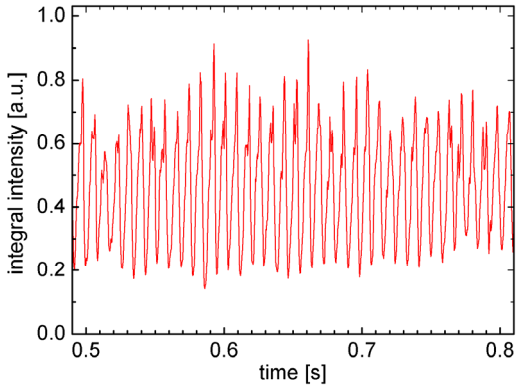

Figure 8 Integral intensity of high-speed OH*-CL images versus recording time for the operating condition with $m_{pf}/m_{pf,ref}$ = 0.75.

oscillation frequency of the CL intensity corresponds very well to the frequency of the measured pressure signal in Fig. 6, as expected.

Flow Fields

The flow field was measured in vertical planes in the combustion chamber. The position of the four planes were defined by the coordinates y = 0, -20, -34, and -39 mm as shown in Fig. 9. They were chosen to cover a large part of the combustion chamber, in particular, the central plane and the plane y = -34 mm that is situated at the edge of the pilot cone (with a diameter of 68 mm) and is crossing approximately the center of two main swirl burners. For selected operating conditions PIV experiments were performed to provide an overview of the flow field and to generate a set of validation data. In Fig. 10 results at the reference operating condition are presented as an example for the overall flow field in the different planes as indicated on the left side of the images. The colors of the 2D images indicate the absolute values of the velocity v and the small arrows the direction. For all planes the averaged values (left side) and the RMS values (right side) are shown. The white line in the averaged image at y = 0 mm

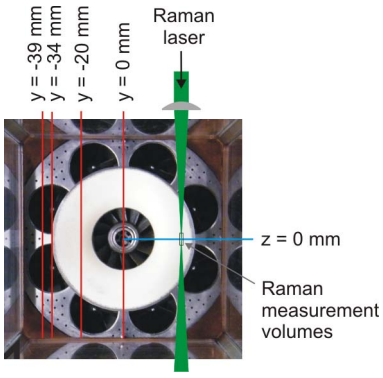

Figure 9. Vertical measuring planes of PIV (red lines) and Raman measurement volume (small rectangle) which was moved to different positions in the horizontal plane z = 0 mm (blue line).

indicates the positions with an axial velocity v_x = 0 m/s. The inner recirculation zone (v_x < 0 m/s) of the pilot burner can be identified in the averaged PIV image of plane y = 0 mm for x < 70 mm whereas the flow of the main burners showed high axial velocity components. The shear layer is visible in the RMS image as the region of higher RMS fluctuations. The flame anchoring region (see Figs. 5 and 11f) lies outside the inner recirculation zone in a region with low to moderate flow velocities. The large RMS velocity fluctuations correspond well with the regions of heat release.

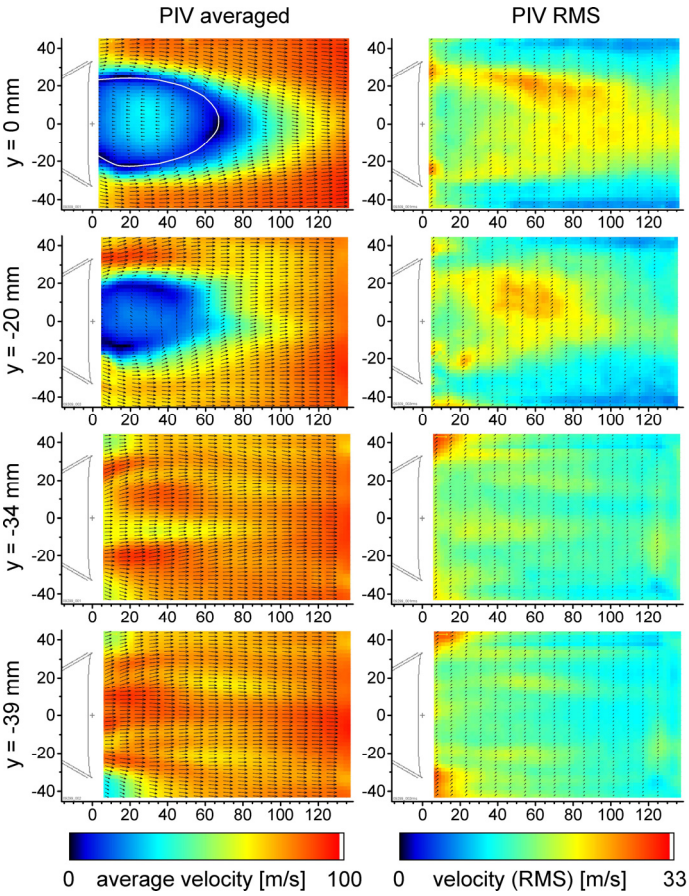

Figure 10. PIV images (left: averages, right: RMS) for different plane positions as indicated on the left side of the images for the reference operating condition. The colors indicate the absolute value of the velocity.

The stagnation point (axial velocity v_x = 0 m/s) was found in the range of 65 mm < x < 70 mm for the reference operating condition (compare Fig. 10, y = 0 mm). Changing the operating condition by reducing the mass flow of the pilot fuel to $m_{pf}/m_{pf,ref}$ = 0.75 the position of the stagnation point increased in x-direction by 7 mm. In case of fuel mixtures of natural gas with hydrogen (40%$_{vol}$ H_2) the flame length becomes shorter and the stagnation point is approximately at 2/3 of the axial position of the reference operating condition.

Major Species Concentrations

The Raman measurements were performed in the horizontal plane z = 0 mm as shown with the blue line in Fig. 9. The one-dimensional resolution of this technique is perpendicular to this plane and covers a length of about ±4 mm in z-direction.

Mixture Fraction and Temperature Statistics: The Raman technique enables the measurement of the instantaneous number densities of the major species and therefore provides insight into the statistical distribution of the local thermochemical state. The scatter plot in Fig. 11a shows the result of such a measurement. It illustrates the correlation of the temperature T with the local mixture fraction f. The dots represent the results obtained from each of the 14 measuring volumes along the laser line for a series of 500 single shot measurements. The blue dots in the plot represent single shot results with H_2O concentrations below 1%$_{vol}$, i.e. unburnt gas at inlet temperature. The blue curve in the graphs represents the estimated mixing temperature of the preheated air and the partially preheated fuel. This temperature was calculated based on the results of thermocouple measurements and flow rate measurements. As the injected fuel was generally colder than the air flow, the mixing temperature slightly decays towards higher mixture fraction values. The red curve in the graphs shows the adiabatic flame temperature as a function of the mixture fraction. The values were calculated using the software GasEq [12]. A solid black line marks the mixture fraction that equals a stoichiometric mixture, while the global mixture fraction (based on flow rate measurements) is indicated by a dashed black line.

A significant variation of the local mixture fraction is reflected by the broad distribution of the blue spots. This fluctuation exceeds the measurement uncertainty by far. Therefore, the variation of f reflects the degree of unmixedness of fuel and air. It is known that a perfect mixing is impossible to achieve under industrial conditions because of the short residence time in the premix region. However, the degree of mixing of fuel and air plays an important role for the combustion behavior, for example for the flame stabilization and NO_x formation. The quality of the mixing and its fluctuations can hardly be measured quantitatively by methods other than Raman scattering.

The five scatter plots of Fig. 11 were recorded at the same axial distance of x = 15 mm from the end of the pilot cone and at the same operating conditions but at different radial distances from the central axis of the combustion chamber y: 40.5, 38, 35, 32, and 30 mm. It can be seen that the frequency of unreacted samples (blue spots), which are typical for the inflow region, decreases towards the central axis. Closer to the central region of the combustion chamber, the statistical distribution becomes dominated by an increasing number of fully reacted samples (red spots) which are defined here by a natural gas concentration of X_{CxHy} < 1%$_{vol}$. At measurement locations close

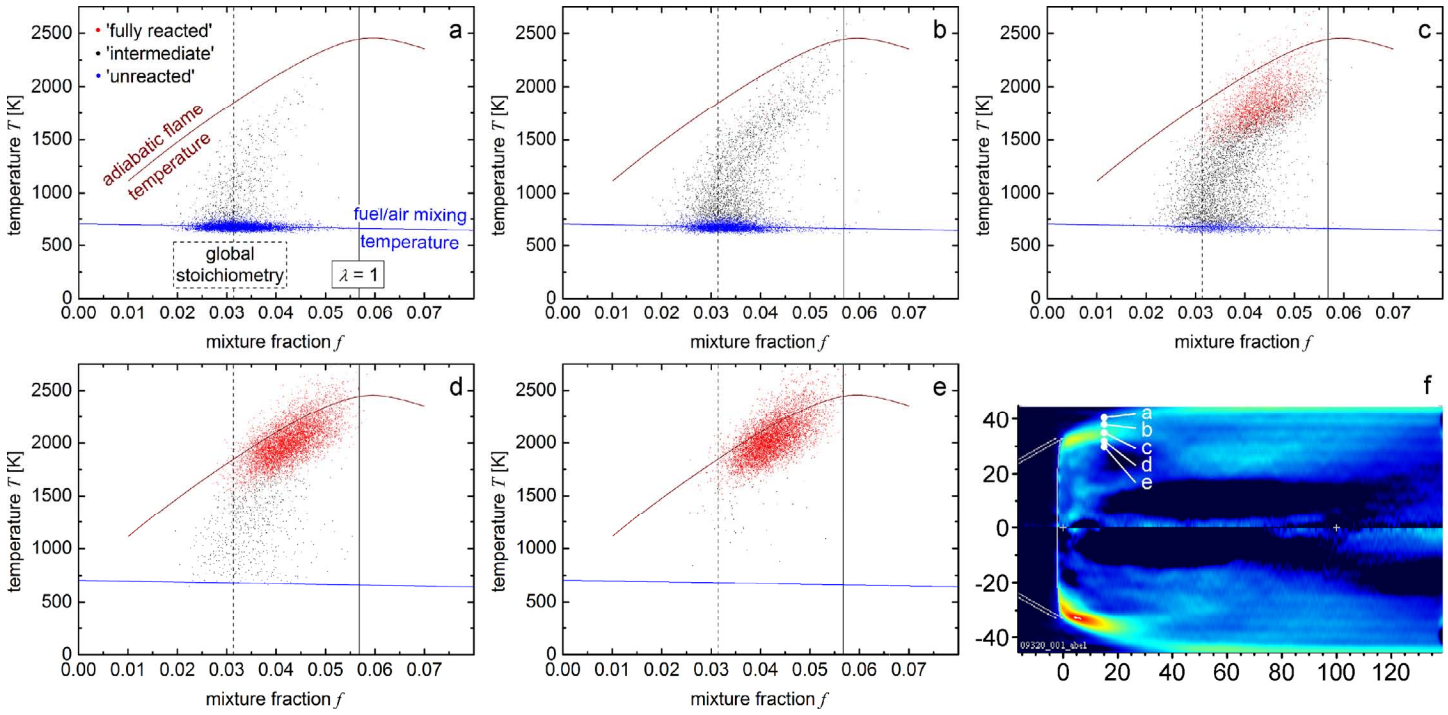

Figure 11. Raman scatter plots for the reference operating condition (a – e, explanations see text). Abel deconvoluted OH*-CL image (f) marked with the measuring positions of the scatter plots a – e (x = 15 mm, y = 40.5 mm, 38 mm, 35 mm, 32 mm, 30 mm, z = 0 mm, respectively).

to the burner, this high fraction of hot reaction products is expected to be stemming mainly from the pilot burner, which also explains the significantly increased mixture fraction of the samples in Fig: 11e compared with the samples in Fig. 11a. The temperature of these fully reacted samples is close to the adiabatic flame temperature. A small portion even exceeds the curve of the adiabatic flame temperature, which can be explained by the limited measurement precision and accuracy. Also, uncertainties of the estimated fuel/air mixing temperature (e.g. systematic deviations of the thermocouple measurements from the real temperature of the fluid) might have an impact on the estimation of the adiabatic flame temperature. Furthermore, there are processes, like heat exchange with the combustion chamber walls that can in fact lead to an additional increase of the gas temperature.

Like other previously performed experiments with Raman spectroscopy at gas turbine flames [4, 13, 14], the results of this campaign reveal a remarkably high frequency of intermediate thermochemical states, which are plotted as black spots in the graphs of Fig. 11. Especially in regions where both components, cold reactants and hot products, are present, such intermediate samples are seen in the measurement results. A good example is Fig. 11c, which represents a measurement recorded at a position in the shear layer between the inflowing cold reactants from the main burner and the flow of hot products from the pilot burner. Interpretations of this phenomenon were already presented in an earlier publication [4]. These come to the conclusion that at least three different effects can cause the observation of intermediate samples:

- The chemical reaction can be interrupted by events of local flame extinction, leaving pockets of partially reacted gas.
- Spatial averaging across the flame front can occur, when the focal region of the laser beam crosses a flame front.
- Regions in which reaction products are very well mixed with unburnt fuel and air may be seen by the measurement before the mixture ignites spontaneously or by flame propagation.

Although, none of these scenarios can be ruled out completely, the first two situations are expected to occur less frequently. Consequently, the largest part of the intermediate samples is likely to be a result of the fast mixing of cold reactants with hot products due to the high turbulence in the shear layers around the inflow region. High strain rates within the shear layers can extend the ignition delay time of such a mixture, which additionally increases the probability of the mixed but unignited state to be captured by a laser shot of the measurement system.

With this interpretation in mind, the scatter plots reflect the mixing and reaction progress in the flame anchoring region.

Mixing of Fuel and Air: As explained above, the high number of single shot spectra which are gained by the 1D Raman technique allow for the quantification of the degree of mixing of fuel and air entering the combustion chamber. A useful quantity that well reflects the level of unmixedness in the flow of reactants is the standard deviation of the mixture fraction calculated only from the statistical population of those samples which were identified as unreacted based on their water concentration. The lower this standard deviation is the

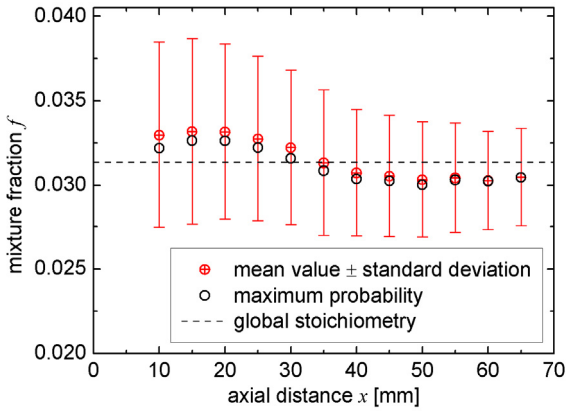

Figure 12. Mixture fraction (mean value, maximum probability and standard deviation) versus the axial distance from the end of the pilot cone.

more homogeneous is the chemical composition of the flow of reactants. In Fig. 12 the standard deviation is plotted as vertical bars around the ensemble averaged mixture fraction of the reactants for 12 different measurement locations. All these measurements were performed at a radial distance of y = 39 mm. Due to the high axial velocity of the inflowing fresh gas, a large fraction of unburnt reactants was found even at locations far downstream. The graph illustrates how the scattering range of the unburnt samples' mixture fraction narrows as the reactants are transported downstream several centimeters. Over the studied path of 55 mm, which corresponds to a flow time scale shorter than 1 ms, the size of the vertical bars is reduced by 47%. This must be interpreted as a process of rapid homogenizing due to turbulent mixing that takes place in the inflow region. According to the authors' knowledge, this is the first time the temporal behavior of the fuel/air mixing quality under GT relevant conditions could be quantified.

Together with the narrowing of the scattering range, the statistical distribution of the mixture fraction in the inflow is becoming more symmetric. The asymmetric statistical distribution of f in the regions close to the burner could already be seen in the distribution of the blue spots in Fig. 11a. There, the highest density of the unreacted samples is slightly offset from the middle of the distribution towards lower mixture fractions. This is reflected more clearly in the deviation of the mixture fraction value with the maximum probability (plotted as open circles) from the mean f value in Fig. 12. This value of maximum probability was determined from the peak position of a Gaussian curve fitted to the mixture fraction histogram of the particular measurement location. The further the reactants flow downstream, the more the offset between these two values decreases, until their merging at x = 65 mm indicates a high symmetry of the f-histogram. This can probably be explained as an effect of the turbulent mixing, too.

Additionally, Fig. 12 shows that the mean local mixture fraction is changing along the investigated axial profile. Close to the burner exit the local mixture tends to be fuel richer than the global mixture fraction, while it is slightly leaner at the downstream axial positions with $x \geq 35$ mm. The fact that this axial profile was located relatively far away from the central axis leads to the assumption that the unreacted samples measured at locations close to the burner only reflect the fuel and the air which was coming from the main burners. Also, the unreacted samples measured far downstream can only originate from the main burner, because the reactants stemming from the pilot burner are expected to be consumed much earlier upstream. In summary, the whole data shown in Fig. 12 is likely to reflect only the flow of fuel and air coming from the main burners. If this conclusion is right, a possible explanation for the spatial variation of the mean mixture fraction could be the existence of fuel rich streaks with a winding three-dimensional shape extending from the main fuel injection holes to the investigated locations.

Instantaneous Profiles of Temperature and Species Concentrations: One advantage of the applied diagnostic method is the one-dimensional spatial resolution which provides instantaneous profiles of the temperature and the concentrations of the major species over a short vertical line of about 8 mm. Single shot series that were recorded in regions where reactants as well as products were present usually result in a large number of instantaneous profiles with steep gradients. Figure 13, for example, shows a single shot from a location close to the measurement position that was chosen for the measurement corresponding to Fig. 11c. In the first millimeter of the investigated line, the chemical composition and the relatively low temperature indicate the presence of unburnt reactants. However, at positions beyond z ≈ -2 mm, the profile reaches values that are typical for the hot products of the fully reacted gas. Between these two parts is a section of about one millimeter in which all plotted scalars drastically change. Whether such a section has to be assigned to a reacting flame front or to a non-reacting mixing layer, cannot be answered unambiguously due to the limited spatial resolution of the diagnostic system. However, the profile was selected out

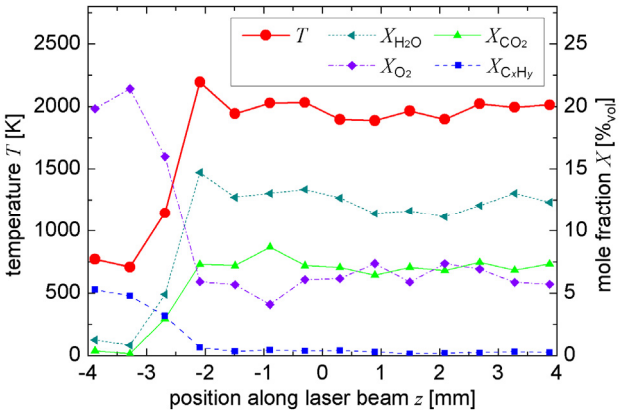

Figure 13. Instantaneous profile of temperature and species concentrations from a single shot one-dimensional Raman measurement.

of a series with 500 single shots as the one with the steepest temperature gradient. It is therefore likely, that the gradient corresponds to a flame front which was intersected nearly perpendicular by the laser beam. One-dimensional simulations of the equilibrium in a premixed counterflow flame (unburnt fuel/air mixture from one side at a velocity of v = 40 m/s, hot reaction products from the other side at a velocity of v = -40 m/s) at slightly different but still comparable conditions (p = 4 bar) were performed using the Cantera code version 1.7 [15]. The maximum temperature gradient in this simulated flame front was 6610 K/mm. In comparison, the temperature gradient in Fig. 13 is about 1700 K/mm. This relatively small value is probably explained by some spatial averaging of the measurement and indicates the spatial resolution achieved in this experiment.

Another way of quantitatively analyzing the spatial information of the instantaneous profiles is to apply an autocorrelation to the single shot profiles. If all 500 correlation functions of one series of single shots are averaged, the result can be used to estimate a turbulent mixing length scale. Approaches of such a kind are currently tested at the DLR and will be subject of future publications.

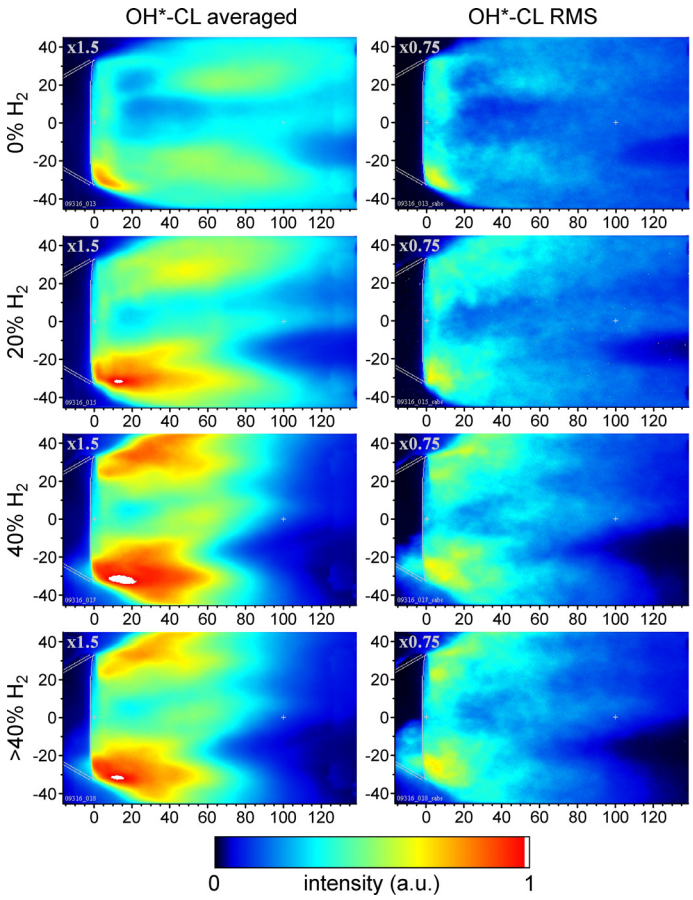

Figure 14. OH*-CL images (left: averages, right: RMS) for different amount of hydrogen admixtures. 0% H_2 referred to the reference operating condition.

Addition of Hydrogen to Main Fuel

To study the capability of fuel flexibility for this combustor experiments were performed in which the natural gas of the main fuel was partly substituted by hydrogen. The adiabatic flame temperature was kept constant in these measurements. Starting from the reference operating condition the hydrogen amount was increased in steps of 10%$_{vol}$. The admixture of 50%$_{vol}$ H_2 could not be reached without the risk of damaging the burner. During the change of the operating condition from 40%$_{vol}$ to 50%$_{vol}$ H_2 a series of OH*-CL images could be recorded and is labeled with ">40% H_2" in Fig. 14. It was found that the NO_x and CO emissions were independent of the hydrogen content for the investigated range up to 40%$_{vol}$ H_2 which is not surprising because the flame temperature was not changed.

In Fig. 14 the OH*-CL images (average and RMS) for different hydrogen contents are presented. The flame length decreased with increasing hydrogen amount, as expected for the higher reactivity of hydrogen. The opening angle of the main flame downstream the pilot cone increased with increasing hydrogen percentage resulting in a movement of the main flame towards the burner. In addition, the flashback probability increased with the hydrogen content. At 20%$_{vol}$ and 30%$_{vol}$ H_2 a flashback event was sometimes observed for a short time. For higher hydrogen amounts (≥40%$_{vol}$) flashbacks occurred quite frequently at different positions. This can be seen in the averaged OH*-CL image but much better in the RMS image in Fig. 14. In the lower left corner CL-signal was observed for x < 0 mm that means upstream of the end of the pilot cone.

SUMMARY AND CONCLUSIONS

A down-scaled staged can combustion system equipped with an optical combustion chamber was successfully operated in the high pressure test rig at DLR in Stuttgart. The main goals of the investigations were a better understanding of the flame stabilization mechanisms and a provision of suitable validation data for CFD models. Different measurement techniques were employed: Exhaust gas analysis, dynamic pressure monitoring, OH* chemiluminescence imaging, particle image velocimetry, and laser Raman scattering. The experiments were performed within a range of relevant operating conditions including variations of the fuel split between pilot and main burners, the flame temperature and the fuel composition. A stably burning flame was chosen as a reference case.

The gas flow from the 8 main burners was ignited by the hot exhaust gas from the central pilot burner. For the reference case, the main flame was anchored at the exit of the pilot burner in the shear layer between the flows from the pilot and main burners. The PIV measurements showed that, on the average, the flow velocities were moderate in this region. The mixing state and reaction progress at this location were characterized by the Raman measurements. Within a small radial region the thermo-chemical state changed from non-

reacted via partially reacted to completely reacted. The partially reacted mixtures are explained by compositions of hot exhaust gas from the pilot flame and fresh fuel/air mixtures from the main burners which were well mixed but have not reacted immediately.

With a reduction of the fuel split, i.e., a decrease of pilot fuel, the flame was no longer anchored at the exit of the pilot burner, but further downstream. At those flame conditions, the flame tended to instabilities in the form of unsteady heat release and thermo-acoustic pulsations.

The Raman measurements revealed that fuel and air were not perfectly premixed before combustion. The degree of unmixedness decreased, as expected, with downstream location. The one-dimensional spatial resolution of the Raman measurements enabled the study of instantaneous profiles of thermochemical scalars. Reaction zones or mixing layers between cold reactants and hot products were clearly visible in these profiles.

With increasing amount of hydrogen in the fuel the flames became shorter, i.e., burnout was faster due to the higher reactivity of H_2. These flames were anchored at the exit of the pilot burner, however, for H_2 amounts larger than $20\%_{vol}$ flashback was occasionally observed. For H_2 amounts larger than $40\%_{vol}$, flashback occurred frequently.

The data set from these measurements comprises much more results than presented in this paper and forms the basis for the validation of numerical simulation methods that will be subject of future publications.

ACKNOWLEDGMENTS

The investigations were conducted as part of the joint research program COORETEC-turbo in the frame of AG Turbo. The work was supported by the Bundesministerium für Wirtschaft und Technologie (BMWi) as per resolution of the German Federal Parliament under grant number 0327716M. The authors gratefully acknowledge AG Turbo and Siemens AG for their support and permission to publish this paper. The responsibility for the content lies solely with its authors.

The authors would like to thank K.-H. Ferst and S. Peukert for the installation as well as U. Prestel and M. Kapernaum for the operation of the combustor and the gas analysis, respectively.

REFERENCES

[1] Gruschka, U., Janus, B. Meisl, J., Huth, M., and Wasif, S., 2008, "ULN System for the New SGT5-8000H Gas Turbine: Design and High Pressure Rig Test Results", In Proc. ASME Turbo Expo 2008, GT2008-51208.

[2] Lee, J.G., and Santavicca, D.A., 2003, "Experimental Diagnostics for the Study of Combustion Instabilities in Lean Premixed Combustors", J. Propulsion and Power **19**, pp. 735-750.

[3] Hardalupas, Y., and Orain, M., 2004, "Local Measurement of the Time-Dependent Heat Release Rate and Equivalence Ratio Using Chemiluminescence Emissions from a Flame", Combust. Flame **139**, pp. 188-207.

[4] Stopper, U., Aigner, M., Ax, H., Meier, W., Sadanandan, R., Stöhr, M., and Bonaldo, A., 2010, „PIV, 2D-LIF and 1D-Raman measurements of flow field, composition and temperature in premixed gas turbine flames", Exp. Thermal Fluid Sci. **34**, pp. 396-403.

[5] Fleck, J., Griebel, P., Steinberg, A., Stöhr, M., and Aigner, M., 2010, „Experimental Investigation of a Generic, Fuel Flexible Reheat Combustor at Gas Turbine Relevant Operating Conditions", In Proc. ASME Turbo Expo 2010, GT2010-22722.

[6] Dandy, D.S., and Vosen, S.R., 1992, "Numerical and Experimental Studies of Hydroxyl Radical Chemo-luminescence in Methane-Air Flames", Combustion Science and Technology **82**, pp. 131 – 150.

[7] Lammel, O., Schütz, H., Schmitz, G., Lückerath, R., Stöhr, M., Noll, B., Aigner, M., Hase, M., and Krebs, W., 2010, „FLOX® Combustion at High Power Density and High Flame Temperatures", In Proc. ASME Turbo Expo 2010, GT2010-23385.

[8] Eckbreth, A., 1996, "Laser Diagnostic for Combustion Temperature and Species", Gordon and Breach .

[9] Barlow, R.S., Carter, C.D., and Pitz, R.W., 2002, "Multiscalar Diagnostics in Turbulent Flames" in "Applied Combustion Diagnostics", Kohse-Höinghaus, K., Jeffries, J. (Eds), Taylor and Francis, New York.

[10] Wehr, L., Meier, M., Kutne, P., and Hassa, C., 2007," Single-pulse 1D laser Raman scattering applied in a gas turbine model combustor at elevated pressure", Proc. Combust. Inst. **31**, pp. 3099–3106.

[11] Bilger, R.W., 1988, "The Structure of Turbulent Non-premixed Flames", Proc. Combust. Inst. **22**, pp. 475-488.

[12] Morley, C., "Gaseq", a chemical equilibrium program for windows, URL `http://gaseq.co.uk`

[13] Ax, H., Stopper, U., Meier, W., Aigner, M., and Güthe, F., "Experimental Analysis of the Combustion Behavior of a Gas Turbine Burner by Laser Measurement Techniques", J. Eng. Gas Turbines Power **132**, Iss. 5, pp. 051503-1 – 051503-9.

[14] Meier, W., Boxx, I., Stöhr, M., and Carter, C.D., 2010, "Laser-based investigations in gas turbine model combustors", Exp. Fluids **49**, pp. 865-882.

[15] Goodwin, D. G. et al., "Cantera", software tools for problems involving chemical kinetics, thermodynamics, and/or transport processes, URL `http://sourceforge.net/projects/cantera`

